Scripta Materialia 177 (2020) 214–217

Contents lists available at ScienceDirect

Scripta Materialia

journal homepage: www.elsevier.com/locate/scriptamat

Local thermal conductivity measurements to determine the fraction of α-cristobalite in thermally grown oxides for aerospace applications

David H. Olson[a], John T. Gaskins[a], John A. Tomko[b], Elizabeth J. Opila[b], Robert A. Golden[c], Gregory J.K. Harrington[c], Adam L. Chamberlain[c], Patrick E. Hopkins[a,b,d,*]

[a] Department of Mechanical and Aerospace Engineering, University of Virginia, Charlottesville, VA 22904, USA
[b] Department of Materials Science and Engineering, University of Virginia, Charlottesville, VA 22904, USA
[c] Rolls-Royce Corporation, Indianapolis, IN 46225, USA
[d] Department of Physics, University of Virginia, Charlottesville, VA 22904, USA

ARTICLE INFO

Article history:
Received 5 September 2019
Revised 15 October 2019
Accepted 17 October 2019

Keywords:
Thermal conductivity
Cristobalite
Thermally grown oxide
Environmental barrier coating
Time-domain thermoreflectance mapping

ABSTRACT

Devitrification of the thermally grown oxide that forms in aerospace coatings used to protect ceramic matrix composites is a contributor to the mechanical failure of these coatings at high operating temperatures. Current methods used to identify the formation of α-cristobalite are time consuming and difficult, due to the limited differences in properties as well as the size scale over which these phase contrasts occur. This study employs time-domain thermoreflectance to spatially profile the thermal conductivity of thermally aged samples, providing a practical method to understand the spatial distribution of α-cristobalite in partially- and fully-devitrified amorphous silica.

Silicon carbide based ceramic matrix composites (SiC CMCs) have entered service as hot section components in gas turbine engines to increase engine efficiency and subsequently reduce emissions. In a combustion environment, SiC CMCs react with water vapor and form a volatile silicon hydroxide gas species ($Si(OH)_4$) [1,2]. This reaction leads to high recession rates of SiC CMCs which necessitates the use of environmental barrier coatings (EBCs) in order to limit the exposure of SiC CMCs to this reaction. The EBC is a multilayer system that typically consists of a silicon layer applied directly to the CMC, and a top coat that has improved stability in the combustion environment. During service, H_2O (g) and O_2 (g) diffuse through the EBC and oxidize the silicon bond coat, resulting in the formation of a protective amorphous silicon dioxide (a-SiO_2) thermally grown oxide (TGO) [3,4]. For long term applications it is desirable to maintain the amorphous TGO; however, the operating temperatures and thermal cycling events of the turbine engine cause the TGO to crystalize into the β-cristobalite polymorph of SiO_2 [5]. The $\beta \rightarrow \alpha$ cristobalite transformation that occurs at $\sim$ 220–270 °C upon cooling is accompanied by a 3–7% volume decrease that results in cracking of the TGO layer [6–8]. The continuous cracking of the TGO layer during service eventually leads to spallation of the EBC [3,9].

Presently, detecting the formation of crystallized portions of amorphous SiO_2 has proven difficult. While analysis using scanning electron microscopy (SEM) and optical microscopy techniques can identify vertical cracks in the TGO, which typically result from the β- to α-cristobalite transformation, quantifying the volume fraction of cristobalite is difficult. Electron backscatter diffraction (EBSD) is ideal for identifying crystalline vs. amorphous regions in the TGO, however, specimen preparation required for this technique can be challenging [10] and generally lacks the capacity for high throughput. While Raman spectroscopy provides a benchmark to identify between the two materials, it lacks the high throughput imaging capabilities as integration of the entirety of the spectra must be performed for a given pixel. The mechanisms of formation and identification of crystalline forms of SiO_2 are paramount to understand the mechanical failure of TGOs. Ultimately this knowledge will drive design and failure criteria for coating systems that form amorphous silica TGOs. In the following study, a thermal conductivity mapping procedure is proposed which takes advantage of the quantifiable differences in thermal conductivity between the varying phases, while offering spatial resolution on the order of several micrometers, allowing for the delineation between a-SiO_2 and α-cristobalite.

* Corresponding author at: Department of Mechanical and Aerospace Engineering, University of Virginia, Charlottesville, VA 22904, USA.
E-mail address: phopkins@virginia.edu (P.E. Hopkins).

https://doi.org/10.1016/j.scriptamat.2019.10.027
1359-6462/

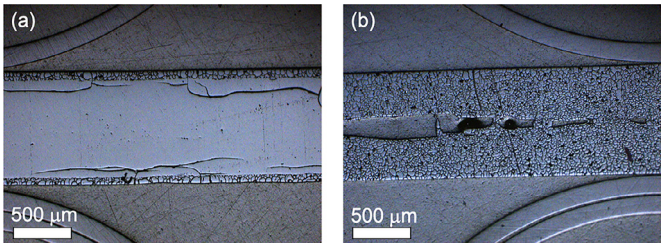

Fig. 1. Optical micrographs of cross-sectioned SiO_2 specimens thermally aged for (a) 100 h and (b) 300 h at 1316 °C.

The thermal conductivity of a-SiO_2 silica is well documented in the literature and typically ranges between 1 and 1.4 W m^{-1} K^{-1} at room temperature [11–14]. On the other hand, the thermal conductivity of α-cristobalite is not as well documented, but is found to range between 3.2 and 5.15 W m^{-1} K^{-1} [15–17]. In general, the thermal conductivity of crystalline solids is larger than those of their amorphous counterparts due to the presence of long-wavelength phonons as the primary heat carriers, compared to more localized modes in amorphous materials that transfer heat via much shorter range vibrational interactions [18]. Despite differences in thermal conductivity, the specific heat capacities remain the same at 741 J g^{-1} K^{-1} [19]. Accounting for the differences in density (2.20 g cm^{-3} for a-SiO_2 [20] and 2.32 g cm^{-3} for α-cristobalite [15]), the volumetric heat capacities are 1.63 and 1.72 MJ m^{-3} K^{-1} for a-SiO_2 and α-cristobalite, respectively. Thus, differences in density between these amorphous and α-cristobalite phases of SiO_2 do not explain the differences in thermal conductivity. The goal of this work is to study the thermal conductivity of α-cristobalite in partially- and fully-devritrified amorphous silica. Using a local measurement technique based on time domain thermroreflectance, thermal conductivity of thermally aged a-SiO_2 was spatially mapped to understand the fraction of α-cristobalite present. Unlike more macroscopic measurements of this crystalline silica phase, local measurements are less prone to obfuscation of the thermal conductivity measurements due to cracking, as these regions can be spatially avoided in the thermal conductivity measurements. Thus, this work provides more robust measurements of the thermal conductivity of fully dense α-cristobalite, in addition to demonstrating the ability to detect the emergence of this crystalline silica phase in a thermally aged TGO.

To observe various levels of devitrification of amorphous silica, high purity a-SiO_2 samples (99.995% pure; Quartz Scientific Inc., Fairport Harbor, OH) were used in this study. Samples were isothermally exposed at 1316 °C for 100 and 300 h in a 90% H_2O – 10% air environment in an alumina tube furnace. Samples were inserted and removed from the tube furnace at temperature. Exposed samples used for time-domain thermoreflectance (TDTR) characterization were mounted in epoxy, cross-sectioned and polished to a 1 μm finish with diamond; the RMS roughness were ~5 nm as measured via mechanical profilometry. Plan-view optical micrographs of the two samples are found in Fig. 1(a) and (b). The exposure to high temperature has a significant effect on the devitrification of the amorphous silica, as evidenced by the noticeable crack formation in Fig. 1(a) and (b). For the 100 h sample, complete devitrification of the glass slide does not occur, and cracks begin to form at the edges of the sample. Cracking occurs throughout the sample exposed for 300 hours.

To confirm the formation of α-cristobalite, Raman spectroscopy was performed on the as-received a-SiO_2 and a reference a-SiO_2 slide isothermally aged at 1316 °C for 100 hours. In their unpolished states, a-SiO_2 remains transparent while α-cristobalite becomes opaque due to cracking. Each specimen was selectively analyzed to confirm the formation of α-cristobalite resulting from the thermal aging process. Excitations were performed at 514 nm, and the acquired Raman spectra are shown in Fig. 2 for the two specimens. Fig. 2(a) shows the Raman spectra for a-SiO_2, which displays numerous broad features associated with the lack of long-range crystalline order. Further, the defect lines, D_1 and D_2, associated with rings in the a-SiO_2 structure, are clearly observed at ~500 and ~600 cm^{-1}, respectively, and labeled in Fig. 2(a) [21]. Similarly, the α-cristobalite Raman spectrum in Fig. 2(b) exhibits a sharp peak at ~421 cm^{-1} due to its six-membered ring structure [22]; this peak is well-defined due to the crystallinity of the sample. Note, another defining peak is present at ~233 cm^{-1}, and is in excellent agreement with prior literature [23]. Both of these peaks arise due to the optical vibrations present in α-cristobalite [24], and are labeled as A_1 in Fig. 2(b). The use of Raman to identify the formation of α-cristobalite at various depths from the edge of the TGO has been shown previously [5]. While this technique identifies the existence of α-cristobalite and offers diffraction-limited spatial resolution, it lacks high throughput imaging capabilities due to integration times associated with each pixel. To further characterize the formation of α-cristobalite, an aluminum film with nominal thickness of 80 nm was deposited on the specimens and TDTR was performed to spatially probe the sample surface in an effort to determine the fraction of α-cristobalite present based on their respective thermal properties.

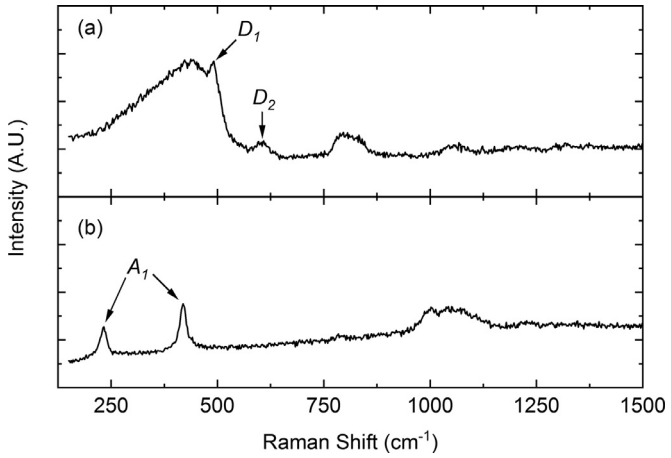

Fig. 2. Raman spectra of the (a) as-received a-SiO_2 slide and (b) reference sample thermally aged at 1316 °C for 100 h. The Raman spectra are indicative of primarily amorphous silica in the as-received glass slide and α-cristobalite in the thermally aged reference sample. Signatures of defect modes are labeled in (a) as D_1 and D_2, while those of optical modes are labeled in (b) as A_1.

TDTR is an optical pump-probe technique that is widely used to characterize the thermal properties of bulk samples and thin films [25–28]. The technique relies on a Ti:Sapphire oscillator with an 80 MHz repetition rate and sub-picosecond pulses. A two-tint setup was employed, where the 808.5 nm output of the oscillator is spectrally separated into a high-energy pump path and a low energy probe path [29]. The pump is electro-optically modulated at 8.4 MHz, creating a frequency-dependent heating event at the sample surface. The probe is mechanically delayed in time and monitors the thermoreflectance at the sample surface. By monitoring the in-phase (V_{in}) and out-of-phase (V_{out}) voltages, and relating the ratio of the two, $-V_{in}/V_{out}$, to the solution to the radially symmetric heat diffusion model [25,26,30,31], various thermal properties can be extracted. An example of the data are shown in Fig. 3, where data and best-fits are shown for spots probed on α-cristobalite and a-SiO_2 portions on the sample exposed at 1316 °C for 100 h. Picosecond acoustics were utilized to derive the thickness of the coated Al layer using the longitudinal speed of sound of 6.24 nm ps^{-1} [20,32,33]. The volumetric heat capacity of α-

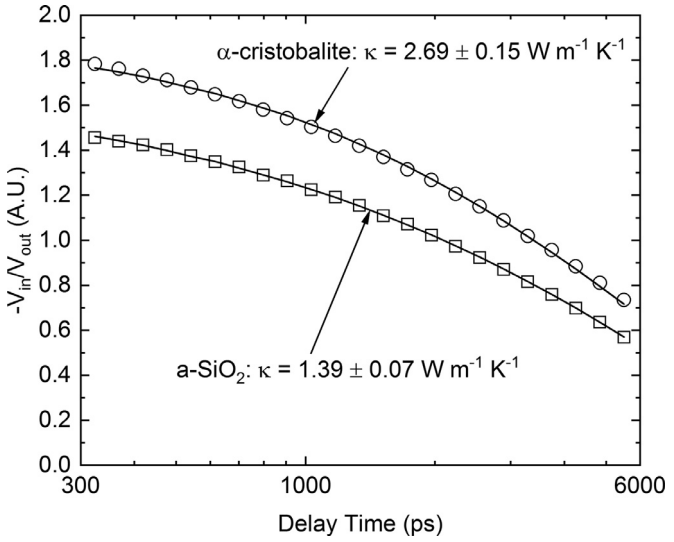

Fig. 3. TDTR ratio of in-phase (V_{in}) to out-of-phase (V_{out}) data and model used to extract the thermal conductivity of amorphous and crystalline regions in the specimen annealed at 1316 °C for 100 h. The open squares and circles are the raw data for the amorphous and crystalline regions, respectively, while the solid lines are the best-fits.

cristobalite and a-SiO_2 were taken to be 1.72 and 1.63 MJ m^{-3} K^{-1}, respectively, as discussed earlier. In all, the thermal conductivity of α-cristobalite and a-SiO_2 are found to be 2.69 ± 0.15 and 1.39 ± 0.07 W m^{-1} K^{-1}, respectively, when performing full TDTR measurements on crystalline and amorphous regions in the sample exposed at 1316 °C for 100 hours. In these and the following measurements, the $1/e^2$ pump and probe radii are ~4.5 and ~3.8 μm, respectively. At these spot sizes, the thermal conductivity of our Al transducer and spot sizes provide a negligible contribution to uncertainty in the extracted thermal conductivity. The uncertainty associated with the reported values reflects multiple measurements over amorphous and crystalline regions, as well as an uncertainty of 2 nm in our Al transducer layer.

The delineation between a-SiO_2 and α-cristobalite, beyond the cracking observed in Fig. 1(a) and (b), is difficult based on the contrasts in conventional optical and scanning electron techniques. The optical contrast in a-SiO_2 vs. α-cristobalite shown in Fig. 1(a) and (b) is negligible, and one would expect a similar lack of contrast from scanning electron micrographs based on the similarities in density. Variations in thermal conductivity are much more tractable based on the large difference between the two phases. Based on acquisition parameters used in this work, the signal to noise ratio of $-V_{in}/V_{out}$ is approximately 25:1, and thus differences in thermal conductivity, and therefore crystallinity, can confidently be observed on the order of 20%.

From a practical standpoint, interrogating a location on a sample using TDTR is time consuming as it is necessary to map out the entire thermal decay curve which often takes several minutes. Various works in the literature have proposed spatially mapping the thermal properties of a given system using pump-probe techniques [34,35], and have specifically shown its applicability on thermal barrier coating systems [36]. This work implements a similar technique. By mounting the sample on a 2-axis stage, the sample is rastered across regions of interest to spatially understand the thermal conductivity in those regions. Due to the fact that the thermal conductivity of a-SiO_2 and α-cristobalite are relatively low, the sensitivity to the boundary conductance between the Al and underlying material is low, allowing a single data point to be taken as an accurate representation of the thermal conductivity of the spot of interest. A pump-probe delay time of 2 ns was utilized, which ensures the results are not influenced by the thermal relaxation time of aluminum while still offering large sensitivity to thermal conductivity of the underlying silica of interest [35,36].

Thermal conductivity maps of the two specimens are shown in Fig. 4, where the pixel size is 2.5 μm. It should be noted that the pixel size used here is dictated by the movement of the travel stage and adjacent pixels, and because of the size of the spot, will inherently sample adjoining pixels. The ratio, $-V_{in}/V_{out}$, is analyzed assuming an average of the volumetric heat capacities of amorphous silica and α-cristobalite for the sample exposed for 100 hours, while that of α-cristobalite is chosen for the sample exposed at 300 h. Maps are originated close to the edge of the epoxy-embedded sample that was exposed at 100 hours to encapsulate as much α-cristobalite as possible, while a spot near the center of the sample aged for 300 h was chosen. Examining Fig. 4(a), a clear difference in thermal conductivity can be observed between the polycrystalline and amorphous regions. For the sample exposed for 100 hours, the thermal conductivity of the amorphous and crystalline regions are determined to be ~1.05 and ~2.50 W m^{-1} K^{-1}. The departure of these values from those discussed earlier can be attributed to the volumetric heat capacity assumed in the analysis. In Fig. 4(c), due to complete devitrification, only the thermal conductivity of α-cristobalite is observed, and a value of 2.75 W m^{-1} K^{-1} is recovered.

Acquisition time of the image is largely dependent on the integration time and filter order of the lock-in amplifier. A time constant of 4 ms and a low-pass filter with a rolloff of 12 dB/oct is used to expedite the mapping process, which correlates to a time per pixel on the order of ~25 ms when each pixel contains 1% of the information from the previous. For a 120 × 120 pixel image, this corresponds to ~10 minutes of acquisition time when accounting for additional waiting considerations. Because the analysis requires solving the heat diffusion equation at a single pump/probe delay time, converting from the ratio ($-V_{in}/V_{out}$) to thermal conductivity takes less than 10 s for 14,400 data points. While thermal conductivity imaging using TDTR can be slower than other techniques that monitor temperature (e.g., full-field spectroscopy [37] and scanning thermal microscopy [38,39]), the ability to extract relevant thermophysical properties beyond just temperature makes the technique unique. Indeed, scanning thermal microscopy offers the capability to extract thermal conductivity on the order of milliseconds per pixel with submicron spatial resolution [40,41], but requires additional sources of uncertainty to be accounted for including goodness of the contact, ballistic conduction via ambient air [42], and the presence of a water meniscus [43], in addition to the complexity of the tip-sample heat transfer process. These sources of uncertainty are not applicable to TDTR.

To better highlight the differences in thermal conductivity, a histogram of the thermal conductivity map from Fig. 4(a) is plotted. A clear difference in the measured thermal conductivity of the two systems is observable in Fig. 4(c). Viewing the thermal conductivity distribution in this way is paramount for understanding the fraction of devitrified silica converted over a particular area. This thermal conductivity technique can be employed to quantify the volume fraction of α-cristobalite in the TGO and relate the volume fraction to coating adherence and/or failure metrics (i.e., bond strength, cycles to failure, etc.).

In summary, an alternative methodology was presented for the identification of α-cristobalite present in devitrified SiO_2 TGOs that forms on silicon bond coats in EBC systems for SiC CMCs. Spatial mapping of the thermal conductivity allows for delineation between α-cristobalite and a-SiO_2 based on the magnitude of the respective thermal conductivities. This method alleviates issues surrounding current methods for identification of α-cristobalite in gas-turbine engine coatings and offers a path forward toward

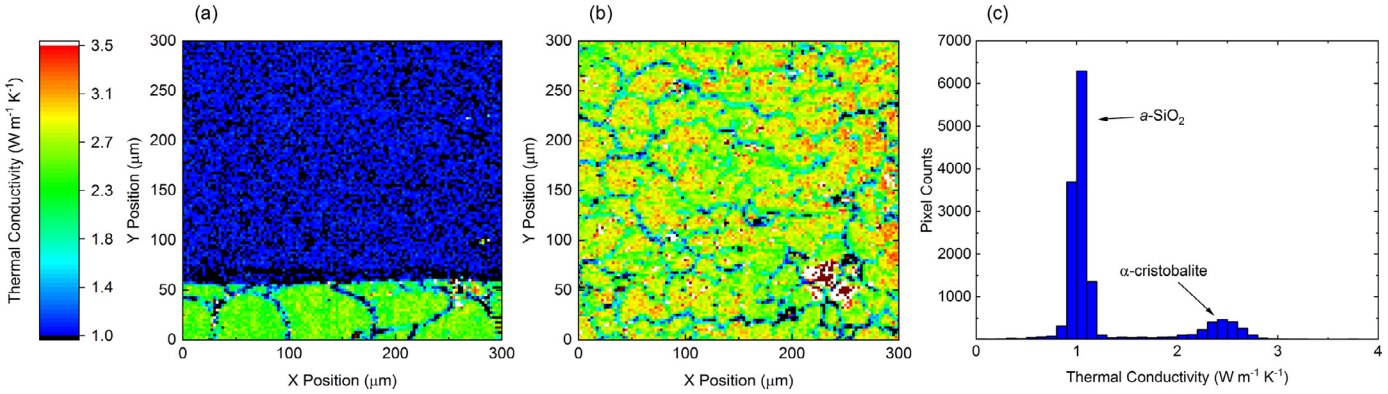

Fig. 4. Thermal conductivity maps of samples annealed for (a) 100 h, and (b) 300 h at 1316 °C. For (a), the map was chosen nearest to the edge of where the sample was embedded into the epoxy, encompassing most of the polycrystalline region possible. In (b), a spot closer to the sample center was chosen. In both maps, a step size of 2.5 μm was chosen. (c) Thermal conductivity distribution from thermal conductivity map in (a). The histogram shows a clear differentiation between the amount of a-SiO_2 and α-cristobalite based on the two thermal conductivity distribution peaks, representative of the respective thermal conductivities of the constituent materials.

further understanding failure mechanisms in these coating systems. Specifically, understanding the fraction of α-cristobalite in a thermally grown oxide presents itself as a quantifiable metric to understand the tolerance level at which α-cristobalite formation helps drive failure in these coatings. Future research will be devoted to the application of this work in relevant coating systems.

Declaration of Competing Interest

The authors declare that they have no known competing financial interests or personal relationships that could have appeared to influence the work reported in this paper.

Acknowledgments

We acknowledge the financial support from Rolls-Royce Corporation (Grant No. 18-UVA-31) and the National Science Foundation (Grant No. CBET-1706388). D. H. Olson is grateful for funding from the National Defense Science and Engineering Graduate (NDSEG) and Virginia Space Grant Consortium (VSGC) Fellowships.

References

[1] E.J. Opila, R.E. Hann, J. Am. Ceram. Soc. 80 (1) (1997) 197–205, doi:10.1111/j.1151-2916.1997.tb02810.x.
[2] E.J. Opila, J.L. Smialek, R.C. Robinson, D.S. Fox, N.J. Jacobson, J. Am. Ceram. Soc. 82 (7) (1999) 1826–1834, doi:10.1111/j.1151-2916.1999.tb02004.x.
[3] B.T. Richards, K.A. Young, F. de Francqueville, S. Sehr, M.R. Begley, H.N. Wadley, Acta Mater. 106 (2016) 1–14, doi:10.1016/J.ACTAMAT.2015.12.053.
[4] K.N. Lee, J. Am. Ceram. Soc. 102 (3) (2019) 1507–1521, doi:10.1111/jace.15978.
[5] B.T. Richards, M.R. Begley, H.N. Wadley, J. Am. Ceram. Soc. 98 (12) (2015) 4066–4075, doi:10.1111/jace.13792.
[6] M.D. Beals, S. Zerfoss, J. Am. Ceram. Soc. 27 (10) (1944) 285–292, doi:10.1111/j.1151-2916.1944.tb14471.x.
[7] D.R. Peacor, Zeitschrift für Kristallographie 138 (1973) 274–298, doi:10.1524/zkri.1973.138.138.274.
[8] P.J. Heaney, C.T. Prewitt, Silica: Physical Behavior, Geochemistry and Materials Applications, Mineralogical Society of America, 1994.
[9] Y. Arai, Y. Aoki, Y. Kagawa, Scr. Mater. 139 (2017) 58–62, doi:10.1016/j.scriptamat.2017.06.006.
[10] W. Wisniewski, S. Berndt, M. Müller, C. Rüssel, CrystEngComm 15 (13) (2013) 2392–2400, doi:10.1039/c3ce26843h.
[11] A.F. Birch, H. Clark, Am. J. Sci. 238 (8) (1940) 529–558, doi:10.2475/ajs.238.8.529.
[12] W.D. Kingery, J. Am. Ceram. Soc. 38 (7) (1955) 251–255, doi:10.1111/j.1151-2916.1955.tb14940.x.
[13] E.H. Ratcliffe, Br. J. Appl. Phys. 10 (1) (1959) 22–25, doi:10.1088/0508-3443/10/1/306.
[14] D.G. Cahill, Rev. Sci. Instrum. 61 (1990) 802, doi:10.1063/1.1141498.
[15] M. Kunugi, N. Soga, H. Sawa, A. Konishi, J. Am. Ceram. Soc. 55 (11) (1972) 580, doi:10.1111/j.1151-2916.1972.tb13442.x.
[16] P. Richet, Y. Bottinga, L. Denielou, J. Petitet, C. Tequi, Geochim. Cosmochim. Acta 46 (12) (1982) 2639–2658, doi:10.1016/0016-7037(82)90383-0.
[17] A.M. Hofmeister, Canad. Mineral. 51 (5) (2013) 705–714, doi:10.3749/canmin.51.5.705.
[18] P.B. Allen, J.L. Feldman, J. Fabian, F. Wooten, Philosoph. Mag. Part B 79 (1999) 1715–1731.
[19] Y.S. Touloukian, E.H. Buyco (Eds.), Thermophysical Properties of Matter – The TPRC Data Series. Volume 5. Specific Heat – Nonmetallic Solids, Plenum, New York, 1970.
[20] D.R. Lide, CRC Handbook of Chemistry and Physics, CRC Press LLC, Boca Raton, 2005.
[21] C. Li, W. Zheng, Q. Zhu, J. Chen, B.Y. Wang, X. Ju, Nuclear Instrum. Methods Phys. Res. Sec. B Beam Interact. Mater. Atoms 384 (2016) 23–29, doi:10.1016/j.nimb.2016.07.018.
[22] K.J. Kingma, R.J. Hemley, Am. Mineralog. 79 (3–4) (1994) 269–273.
[23] J.B. Bates, J. Chem. Phys. 57 (9) (2004) 4042–4047, doi:10.1063/1.1678878.
[24] J.F. Scott, S.P.S. Porto, Phys. Rev. 161 (3) (1967) 903–910, doi:10.1103/PhysRev.161.903.
[25] D.G. Cahill, Rev. Sci. Instrum. 75 (12) (2004) 5119–5122, doi:10.1063/1.1819431.
[26] P.E. Hopkins, J.R. Serrano, L.M. Phinney, S.P. Kearney, T.W. Grasser, C.T. Harris, J. Heat Transf. 132 (8) (2010) 81302, doi:10.1115/1.4000993.
[27] J. Liu, J. Zhu, M. Tian, X. Gu, A. Schmidt, R. Yang, Rev. Sci. Instrum. 84 (2013) 034902, doi:10.1063/1.4797479.
[28] P. Jiang, X. Qian, R. Yang, J. Appl. Phys. 124 (16) (2018) 161103, doi:10.1063/1.5046944.
[29] K. Kang, Y.K. Koh, C. Chiritescu, X. Zheng, D.G. Cahill, Rev. Sci. Instrum. 79 (2008) 114901, doi:10.1063/1.3020759.
[30] A.J. Schmidt, X. Chen, G. Chen, Rev. Sci. Instrum. 79 (11) (2008) 114902, doi:10.1063/1.3006335.
[31] J.L. Braun, P.E. Hopkins, J. Appl. Phys. 121 (2017) 175107, doi:10.1063/1.4982915.
[32] C. Thomsen, H.J. Maris, J. Tauc, Thin Solid Films 154 (1) (1987) 217–223, doi:10.1016/0040-6090(87)90366-X.
[33] K.E. O'hara, X. Hu, D.G. Cahill, Nanoscale Therm. Transp. J. Appl. Phys. 90 (4852) (2001) 793, doi:10.1063/1.1406543.
[34] S. Huxtable, D.G. Cahill, V. Fauconnier, J.O. White, J.C. Zhao, Nat. Mater. 3 (5) (2004) 298–301, doi:10.1038/nmat1114.
[35] C. Wei, X. Zheng, D.G. Cahill, J.C. Zhao, Rev. Sci. Instrum. 84 (2013) 71301, doi:10.1063/1.4815867.
[36] X. Zheng, D.G. Cahill, J.C. Zhao, Adv. Eng. Mater. 7 (7) (2005) 622–626, doi:10.1002/adem.200500024.
[37] G. Tessier, M. Bardoux, C. Boú, C. Filloy, D. Fournier, Appl. Phys. Lett. 90 (17) (2007) 1–4, doi:10.1063/1.2732179.
[38] S. Gomes, A. Assy, P.O. Chapuis, Phys. Status Solid. a 212 (3) (2015) 477–494, doi:10.1002/pssa.201400360.
[39] A. Majumdar, Ann. Rev. Mater. Sci. 29 (1999) 505–585.
[40] H.H. Roh, J.S. Lee, D.L. Kim, J. Park, K. Kim, O. Kwon, S.H. Park, Y.K. Choi, A. Majumdar, J. Vacuum Sci. Technol. B Microelectron. Nanometer Struct. 24 (5) (2006) 2405–2411, doi:10.1116/1.2353843.
[41] H.H. Roh, J.S. Lee, D.L. Kim, J. Park, K. Kim, O. Kwon, S.H. Park, Y.K. Choi, A. Majumdar, J. Vacuum Sci. Technol. B Microelectron. Nanometer Struct. 24 (5) (2006) 2398–2404, doi:10.1116/1.2353842.
[42] K. Kim, J. Chung, G. Hwang, O. Kwon, J.S. Lee, ACS Nano 5 (11) (2011) 8700–8709, doi:10.1021/nn2026325.
[43] S. Lefèvre, S. Volz, P.O. Chapuis, Int. J. Heat Mass Transf. 49 (1–2) (2006) 251–258, doi:10.1016/j.ijheatmasstransfer.2005.07.010.